High-Speed Mid-Wave Infrared Uni-Traveling Carrier Photodetector Based on InAs/InAsSb Type-II Superlattice

Jian Huang, Zhijian Shen, Zongti Wang, Zhiqi Zhou, Ziyu Wang, Bo Peng, Weimin Liu, Yiqiao Chen, and Baile Chen, *Senior Member, IEEE*

***Abstract*— High-speed photodetectors operating at mid-wave infrared are crucial for free-space optical communication and frequency comb spectroscopy. In this letter, we report a high-speed mid-wave infrared uni-traveling carrier photodiode based on InAs/InAsSb type-II superlattice at room temperature for the first time. The device exhibits a cut-off wavelength of around 5.5 μm at room temperature. The responsivity of the device is about 0.6 A/W (at 4.5 μm) under −1 V at room temperature. The frequency response of the device is characterized by an optical parametric amplification system generating mid-infrared femtosecond pulses. A device with a 20 μm diameter has a 3-dB bandwidth of 12.8 GHz at −4 V. These promising results suggest that the device could be potential candidates to be employed in the emerging high-speed MWIR applications.**

***Index Terms*— Uni-traveling carrier photodiodes, high speed photodetectors, mid-wavelength infrared photodetectors, InAs/InAsSb type II superlattices.**

I. Introduction

MID-WAVE infrared (MWIR) (3-5 μm) photodetectors (PDs) have been widely used in many applications such as chemical sensing, imaging, and target tracking over the past several decades. In recent years, thanks to the development of quantum cascade laser (QCL) [1] and interband cascade laser (ICL) [2] technology, the requirements of high-speed MWIR photodetectors are growing rapidly in different fields like free-space optical communication [3] and frequency comb spectroscopy [4], [5]. Thus, it has attracted intense interest in high-speed MWIR photodetectors study recently. Quantum cascade detectors (QCDs) [6], [7], interband cascade infrared photodetectors (ICIPs) [8]–[11], and quantum well infrared photodetectors (QWIPs) [12] based high-speed MWIR photodetectors have been demonstrated in the mainstream. Nevertheless, QCDs suffer from low responsivity [13] due to the multiple-stage architecture and considerably lower carrier lifetimes, while QWIPs are limited by the large dark current [12]. Hence, high-speed MWIR photodetectors based on other device structures and material systems need further developments [14].

Antimonide-based type-II superlattices (T2SLs) have been recognized as a promising candidate for infrared photodetectors due to the tunable energy bandgap, which can cover from short-wave infrared to long-wave infrared range [15]. Besides, compared with traditional mercury cadmium telluride (HgCdTe), antimonide-based Type-II superlattices also enjoy the advantages of low auger recombination rates, high material uniformity, and high operating temperature [16]. Among them, Ga-free InAs/InAsSb T2SL has emerged as a versatile infrared photodetector material in recent years. It has been reported that InAs/InAsSb T2SLs have a longer minority carrier lifetime compared to InAs/GaSb T2SLs, which can achieve high quantum efficiency (QE) and work at a higher temperature [17], [18]. Besides, InAs/InAsSb T2SL has a relatively simple interface structure, benefiting from more manageable material growth. Several works have demonstrated high-performance MWIR or LWIR photodetectors based on InAs/InAsSb T2SLs [19]–[22]. So far, the bandwidth performance of InAs/InAsSb T2SL photodetectors has not been reported yet.

This letter demonstrates a high-speed InAs/InAsSb T2SL MWIR photodiode based on uni-traveling carrier (UTC) structure at room temperature. In the UTC structure, the photo-generate carriers are produced in the p-type absorber region [23]. The photo-generate holes can quickly be collected within dielectric relaxation time, and only electrons are

Manuscript received March 14, 2022; accepted March 28, 2022. Date of publication March 31, 2022; date of current version April 26, 2022. This work was supported in part by the National Key Research and Development Program of China under Grant 2018YFB2201000 and in part by the National Natural Science Foundation of China under Grant 61975121. The review of this letter was arranged by Editor L. K. Nanver. *(Corresponding author: Baile Chen.)*

Jian Huang is with the School of Information Science and Technology, ShanghaiTech University, Shanghai 201210, China, also with the Shanghai Institute of Microsystem and Information Technology, Chinese Academy of Sciences, Shanghai 200050, China, and also with the University of Chinese Academy of Sciences, Beijing 100049, China.

Zhijian Shen, Zongti Wang, and Zhiqi Zhou are with the School of Information Science and Technology, ShanghaiTech University, Shanghai 201210, China.

Ziyu Wang, Bo Peng, and Weimin Liu are with the School of Physical Science and Technology, ShanghaiTech University, Shanghai 201210, China.

Yiqiao Chen is with Acken Optoelectronic Ltd., Suzhou 215212, China, and also with the Shanghai Institute of Microsystem and Information Technology, Chinese Academy of Sciences, Shanghai 200050, China.

Baile Chen is with the School of Information Science and Technology, ShanghaiTech University, Shanghai 201210, China, and also with the Shanghai Engineering Research Center of Energy Efficient and Custom AI IC, Shanghai 201210, China (e-mail: chenbl@shanghaitech.edu.cn).

Color versions of one or more figures in this letter are available at https://doi.org/10.1109/LED.2022.3163660.

Digital Object Identifier 10.1109/LED.2022.3163660

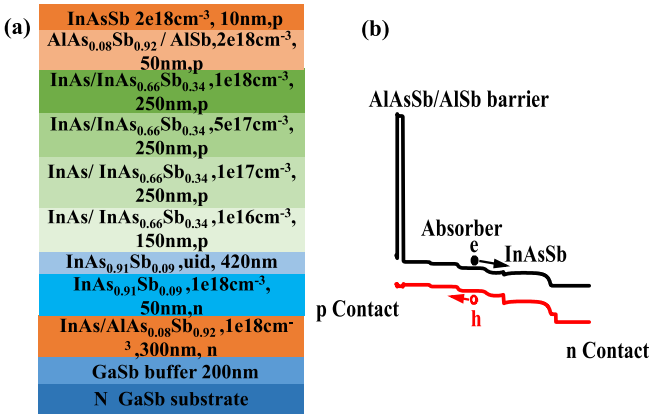

Fig. 1. (a) Epitaxial structure of the device. (b) Schematic band diagram of the device.

injected into drift layers. Thus the total carrier transit time of the device is shorter than that of traditional PIN photodetectors. It is expected to have better bandwidth. Given the typically significant difference between electron mobility and hole mobility in InAs/InAsSb T2SLs [24], it is anticipated that the UTC structure could outperform the PIN structure in terms of the device bandwidth. In this work, the bandwidth performance of the device is characterized by a femtosecond MWIR pulse. The cut-off wavelength of the device is about 5.5 μm at room temperature, and the responsivity (at 4.5 μm) is about 0.6 A/W at -1 V. The 3-dB bandwidth of a 20 μm diameter detector is about 12.8 GHz at -4V. This is the highest value reported among any Sb-based photodetectors working in the MWIR range.

II. Device Growth and Fabrication

Fig. 1(a) shows the epitaxial structure of the designed device. The structure was grown on an n-type GaSb substrate by molecular beam epitaxy system (MBE). The epitaxial growth started with a 200 nm thick GaSb buffer followed by a 300 nm InAs/AlAsSb (1.5 nm/1.5nm) SL bottom contact layer and 50 nm n-type InAsSb. After that, a 420 nm thick un-intentionally doped (u.i.d.) InAsSb drift layer was grown, followed by InAs/InAsSb (2.9 nm/1 nm) SL absorption layer with four-step graded doping. Here, in order to balance the responsivity and bandwidth of the device, the total thickness of absorber was set to 900 nm. Then, a 50 nm thick AlAsSb/AlSb (1.22 nm/0.61 nm) SL electron barrier was grown. Finally, a 10 nm thick InAsSb top contact layer was used to cap the structure. Fig. 1(b) shows the schematic energy band diagram of the UTC PD.

After material growth, the sample was processed into circle mesa-shaped devices. Standard photolithography and inductively coupled plasma (ICP) dry etch were used to define the mesa. Ti/Pt/Au metals were deposited on the top and bottom contact layers to form ohmic contact through e-beam evaporation. SU-8 photoresist was used to passivate the mesa surface. For the high-frequency test, the device was connected to a coplanar waveguide (CPW) pad of 50 Ω characteristic impedance through an air bridge by electroplating [25].

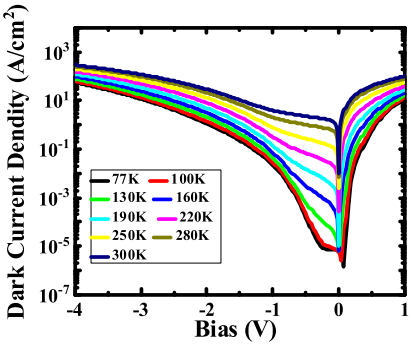

Fig. 2. Dark current density as a function of bias of the device under different temperatures.

III. Results and Discussion

Fig. 2 shows the measured dark current density (J-V) of a device with diameter of 20 μm as a function of bias voltage for temperature ranging from 77 K to 300 K. As temperature rises from 77 K to 300 K, the dark current density increases from 0.02 A/cm^2 to 3.94 A/cm^2 at -1 V. With bias further increases, tunneling current becomes evidently. Fig. 3(a) presents the Arrhenius plot of temperature-dependent dark current density under -0.5 V. The linear fit at 220 K-300 K yields an activation energy of 248 meV, which is very close to the effect bandgap energy of InAs/InAsSb SL absorption layer, indicating that the diffusion component dominates the dark current of the device. At 160 K to 220 K, the activation energy decreases to 157 meV, suggesting that the dark current of the device is dominated by both diffusion and generation-recombination (G-R) mechanisms. When the temperature is below 130 K, a small activation energy value of 21 meV indicates tunneling component dominated dark current.

The photo-response of the top-illuminated device was measured by a Fourier transform infrared spectrometer (FTIR) and calibrated by a blackbody source without any anti-reflection (AR) coating. Fig. 3(b) shows the responsivity of the device at different temperatures under zero bias. The cut-off wavelength is about 5.5 μm at 300 K for the device. The peak responsivity at 77 K is about 0.88 A/W at around 3.61 μm. As temperature rises, the responsivity of first stays at a similar level at 77 K to 220 K. Once the temperature goes up to above 220K, the responsivity decreases gradually. Fig. 3(c) shows the responsivity of the device under different biases at 300 K. As bias rises from 0 V to -1 V, the responsivity quickly increases, the responsivity at 3 μm under -1V is around 0.8 A/W. In contrast, the responsivity at 5μm is approximately 0.2 A/W. The Johnson-noise and shot-noise-limited detectivity under different biases at 300 K has also been calculated and shown in Fig. 3(d). The peak detectivity of the device is about 3×10^8 Jones at 0V and increases to 7×10^8 Jones at -1V. These detectivity values are slightly lower than the recent reported InAs/InAsSb type-II SL photodiodes [19], [26], which is probably due to the reduced carrier lifetime in the highly p- doped in SLs.

For the high-speed performance characterization, an optical parametric amplification (OPA) system (Coherent, Inc. OPerA Solo) was used to characterize the device. The OPA system was pumped by a Ti: sapphire laser (Coherent, Inc.

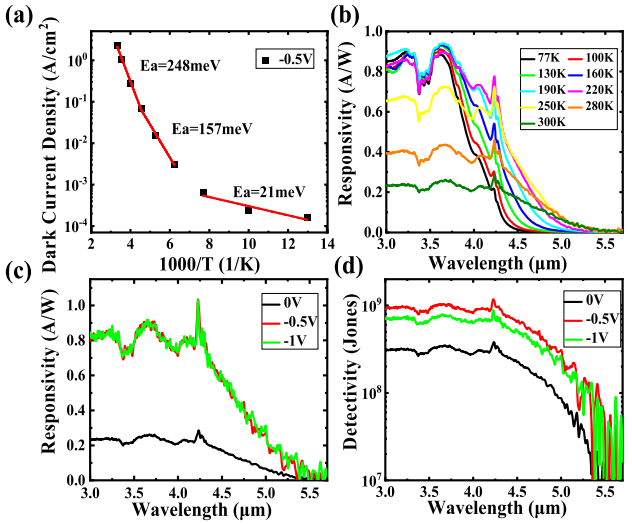

Fig. 3. (a) Arrhenius plots and the linear fits of dark current density of the device under −0.5V. (b) Responsivity of the device under zero bias at different temperatures. (c) Responsivity of the device under different biases at 300 K. (d) Johnson-noise and shot-noise-limited detectivity of the device under different biases at 300 K.

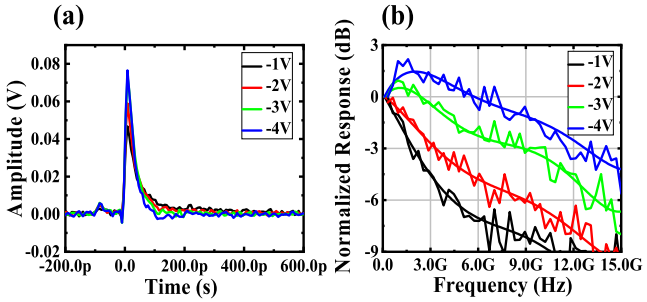

Fig. 4. (a) Pulse response of the device under different biases at room temperature. (b) The normalized frequency response of the device under different biases at room temperature.

Astrella USP) with a pulse repetition rate of 1 kHz and a full-width at half-maximum (FWHM) pulse duration of 38 fs. The MWIR pulses were generated by a wavelength-tunable femtosecond pulsed OPA and coupled to the device under test (DUT) by a focus lens. A GSG probe collected the photo-response of the device, and a bias tee separated the RF and DC components of the electrical signal. The RF signal was recorded by a real-time digital oscilloscope (Keysight Infiniium DSAZ594A), and the DC part was connected to a source meter.

Fig. 4(a) shows the pulse response of the device with a diameter of 20 μm under different biases at room temperature. Here, we measured the pulse response by tuning the wavelength of OPA around 5 μm. As shown in Fig. 4(a), as the bias rises, the amplitude of the electrical pulse increases. At −3 V, the pulse response of the device has a FWHM of about 30 ps. The frequency response of the device can be derived from the Fourier transform of pulse response, with the loss of used RF cable, GSG probe, and Bias-T carefully calibrated. Fig. 4(b) shows the normalized frequency response of the device. As bias increases from −1 V to −2 V, the 3-dB bandwidth changes from 2.02 GHz to 3.42 GHz. With bias further increasing to −3 V, the 3-dB bandwidth rises to 8.85 GHz and quickly reaches to12.8 GHz at −4 V.

TABLE I
PERFORMANCE COMPARISON OF HIGH SPEED MWIR PHOTODETECTORS AT 300 K

Ref	Device structure	Cut-off Wavelength (μm)	Responsivity (A/W)	Dark current density (A/cm²)	3dB bandwidth (GHz)
[12]	QWIP	4.9	0.1(-5V)	80(-5V)	5(-4V)
[6]	QCD	4.3	0.008(0V)	NA	21(0V)
[7]	QCD	4.5	0.0065(0V)	NA	23(0V)
[13]	QCD	4.3	0.0078(0V)	NA	9(0V)
[8]	ICIP	4.2	0.2(0V) @3.15μm	0.2(-1V)	1.3(0V)
[9]	ICIP	5.3	0.1(0V) @4.5μm	10(-1V) 20(-5V)	0.17(-1V) 2.4(-5V)
[11]	ICIP	5	0.067(-0.3V) @ 3.5μm	0.3(-1V) 1.04(-5V)	0.91(-1V) 7.04(-5V)
[27]	PIN	5.33	1.8 (77K@4.35μm)	7(77K, -2.5V)	8.5(-2.5V)
[25]	UTC	5.6	0.05(0V) @4.5μm	0.65(-1V) 6.5(-5V)	2.25(-1V) 6.58(-5V)
This work	UTC	5.5	0.17(0V)@4.5 μm 0.6(-1V)@4.5 μm	3.94(-1V) 296(-4V)	2.02(-1V) 12.8(-4V)

The performance comparison of the InAs/InAsSb UTC device with other high-speed MWIR photodiodes has been listed in Table I. As shown in Table I, QCDs can achieve more than 20 GHz bandwidth due to the fast electrons tunneling time and intersubband scattering process [7]. However, the responsivity of QCDs is only around 10 mA/W. The reported QWIP needs high bias and suffers from low responsivity and large dark current [12]. For ICIP, the short carrier transit time in one cascade stage contributes to high-speed operation. However, the balance between bandwidth and responsivity needs further investigation to improve the devices' performance [8], [9], [11]. InSb based PIN PD with a 3-dB bandwidth of 8.5 GHz has also been reported [26]. Nevertheless, the significant dark current limits it to work under low temperatures. Compared with these works, our device shows much higher responsivity and has a broad band respnse. The bandwidth of our device is better than ICIPs and comparable to that of QCD at high bias. The overall performance of our device at low bias is better than ICIPs in [9] and [11] and similar to that in [8]. In addition, compared to the InAs/GaSb type-II SL based UTC PD [25], our device also has the advantage in responsivity and bandwidth. However, there is still a remaining problem associated with our devices' large dark current at high bias. Further works are needed to operate the devices at lower bias such as reducing the background doping of the InAsSb collector layers.

IV. CONCLUSION

In summary, we have demonstrated high-speed InAs/InAsSb T2SL MWIR photodetector based on uni-traveling carrier design at room temperature. The device exhibits a cut-off wavelength of about 5.5 μm at room temperature, and the responsivity (at 4.5 μm) is about 0.6 A/W at −1 V. The 3-dB bandwidth of a 20 μm diameter detector is about 12.8 GHz at −4V. We believe this InAs/InAsSb T2SL based PD has great potential for high-speed applications with further performance improvement.

REFERENCES

[1] W. Zhou, S. Slivken, and M. Razeghi, "Phase-locked, high power, mid-infrared quantum cascade laser arrays," *Appl. Phys. Lett.*, vol. 112, no. 18, Apr. 2018, Art. no. 181106.

[2] J. Hillbrand, M. Beiser, A. M. Andrews, H. Detz, R. Weih, A. Schade, S. Höfling, G. Strasser, and B. Schwarz, "Picosecond pulses from a mid-infrared interband cascade laser," *Optica*, vol. 6, no. 10, pp. 1334–1337, 2019.

[3] C. Liu, S. Zhai, J. Zhang, Y. Zhou, Z. Jia, F. Liu, and Z. Wang, "Free-space communication based on quantum cascade laser," *J. Semicond.*, vol. 36, no. 9, Sep. 2015, Art. no. 094009.

[4] B. Meng, M. Singleton, M. Shahmohammadi, F. Kapsalidis, R. Wang, M. Beck, and J. Faist, "Mid-infrared frequency comb from a ring quantum cascade laser," *Optica*, vol. 7, no. 2, pp. 162–167, 2020.

[5] A. Hugi, G. Villares, S. Blaser, H. C. Liu, and J. Faist, "Mid-infrared frequency comb based on a quantum cascade laser," *Nature*, vol. 492, no. 7428, pp. 229–233, Dec. 2012.

[6] J. Hillbrand, L. M. Krüger, S. D. Cin, H. Knötig, J. Heidrich, A. M. Andrews, G. Strasser, U. Keller, and B. Schwarz, "High-speed quantum cascade detector characterized with a mid-infrared femtosecond oscillator," *Opt. Exp.*, vol. 29, no. 4, pp. 5774–5781, 2021.

[7] T. Dougakiuchi, A. Ito, M. Hitaka, K. Fujita, and M. Yamanishi, "Ultimate response time in mid-infrared high-speed low-noise quantum cascade detectors," *Appl. Phys. Lett.*, vol. 118, no. 4, Jan. 2021, Art. no. 041101.

[8] H. Lotfi, L. Li, L. Lei, H. Ye, S. M. S. Rassel, Y. Jiang, R. Q. Yang, T. D. Mishima, M. B. Santos, J. A. Gupta, and M. B. Johnson, "High-frequency operation of a mid-infrared interband cascade system at room temperature," *Appl. Phys. Lett.*, vol. 108, no. 20, May 2016, Art. no. 201101.

[9] Y. Chen, X. Chai, Z. Xie, Z. Deng, N. Zhang, Y. Zhou, Z. Xu, J. Chen, and B. Chen, "High-speed mid-infrared interband cascade photodetector based on InAs/GaAsSb type-II superlattice," *J. Lightw. Technol.*, vol. 38, no. 4, pp. 939–945, Feb. 15, 2020.

[10] L. M. Krüger, J. Hillbrand, J. Heidrich, M. Beiser, R. Weih, J. Koeth, C. R. Phillips, B. Schwarz, G. Strasser, and U. Keller, "High-speed interband cascade infrared photodetectors: Photo-response saturation by a femtosecond oscillator," *Opt. Exp.*, vol. 29, no. 9, pp. 14087–14100, 2021.

[11] Z. Xie, J. Huang, X. Chai, Z. Deng, Y. Chen, Q. Lu, Z. Xu, J. Chen, Y. Zhou, and B. Chen, "High-speed mid-wave infrared interband cascade photodetector at room temperature," *Opt. Exp.*, vol. 28, no. 24, pp. 36915–36923, 2020.

[12] E. Rodriguez, A. Mottaghizadeh, D. Gacemi, D. Palaferri, Z. Asghari, M. Jeannin, A. Vasanelli, A. Bigioli, Y. Todorov, M. Beck, J. Faist, Q. J. Wang, and C. Sirtori, "Room-temperature, wide-band, quantum well infrared photodetector for microwave optical links at 4.9 μm wavelength," *ACS Photon.*, vol. 5, no. 9, pp. 3689–3694, Sep. 2018.

[13] Y. Zhou, S. Zhai, F. Wang, J. Liu, F. Liu, S. Liu, J. Zhang, N. Zhuo, L. Wang, and Z. Wang, "High-speed, room-temperature quantum cascade detectors at 4.3 μm," *AIP Adv.*, vol. 6, no. 3, Mar. 2016, Art. no. 035305.

[14] B. Chen, Y. Chen, and Z. Deng, "Recent advances in high speed photodetectors for eSWIR/MWIR/LWIR applications," *Photonics*, vol. 8, no. 1, p. 14, Jan. 2021. [Online]. Available: https://www.mdpi.com/2304-6732/8/1/14

[15] M. Razeghi and B.-M. Nguyen, "Band gap tunability of type II antimonide-based superlattices," *Phys. Proc.*, vol. 3, no. 2, pp. 1207–1212, 2010.

[16] M. Razeghi, A. Haddadi, A. M. Hoang, G. Chen, S. Bogdanov, S. R. Darvish, F. Callewaert, P. R. Bijjam, and R. McClintock, "Antimonide-based type II superlattices: A superior candidate for the third generation of infrared imaging systems," *J. Electron. Mater.*, vol. 43, no. 8, pp. 2802–2807, 2014.

[17] E. H. Steenbergen, B. C. Connelly, G. D. Metcalfe, H. Shen, M. Wraback, D. Lubyshev, Y. Qiu, J. M. Fastenau, A. W. K. Liu, S. Elhamri, O. O. Cellek, and Y.-H. Zhang, "Significantly improved minority carrier lifetime observed in a long-wavelength infrared III–V type-II superlattice comprised of InAs/InAsSb," *Appl. Phys. Lett.*, vol. 99, no. 25, Dec. 2011, Art. no. 251110.

[18] B. V. Olson, E. A. Shaner, J. K. Kim, J. F. Klem, S. D. Hawkins, L. M. Murray, J. P. Prineas, M. E. Flatté, and T. F. Bogges, "Time-resolved optical measurements of minority carrier recombination in a mid-wave infrared InAsSb alloy and InAs/InAsSb superlattice," *Appl. Phys. Lett.*, vol. 101, no. 9, 2012, Art. no. 092109.

[19] D. Wu, J. Li, A. Dehzangi, and M. Razeghi, "High performance InAs/InAsSb type-II superlattice mid-wavelength infrared photodetectors with double barrier," *Infr. Phys. Technol.*, vol. 109, Sep. 2020, Art. no. 103439.

[20] D. Wu, J. Li, A. Dehzangi, and M. Razeghi, "Mid-wavelength infrared high operating temperature pBn photodetectors based on type-II InAs/InAsSb superlattice," *AIP Adv.*, vol. 10, no. 2, Feb. 2020, Art. no. 025018.

[21] G. Deng, D. Chen, S. Yang, C. Yang, J. Yuan, W. Yang, and Y. Zhang, "High operating temperature pBn barrier mid-wavelength infrared photodetectors and focal plane array based on InAs/InAsSb strained layer superlattices," *Opt. Exp.*, vol. 28, no. 12, pp. 17611–17619, 2020.

[22] D. Z. Ting, A. Soibel, A. Khoshakhlagh, S. A. Keo, A. M. Fisher, S. B. Rafol, L. Höglund, C. J. Hill, B. J. Pepper, and S. D. Gunapala, "Long wavelength InAs/InAsSb superlattice barrier infrared detectors with p-type absorber quantum efficiency enhancement," *Appl. Phys. Lett.*, vol. 118, no. 13, Mar. 2021, Art. no. 133503.

[23] Y. Chen, Z. Xie, J. Huang, Z. Deng, and B. Chen, "High-speed uni-traveling carrier photodiode for 2 μm wavelength application," *Optica*, vol. 6, no. 7, pp. 884–889, 2019.

[24] A. Soibel, D. Z. Ting, A. M. Fisher, A. Khoshakhlagh, B. Pepper, and S. D. Gunapala, "Temperature dependence of diffusion length and mobility in mid-wavelength InAs/InAsSb superlattice infrared detectors," *Appl. Phys. Lett.*, vol. 117, no. 23, Dec. 2020, Art. no. 231103.

[25] J. Huang, Z. Xie, Y. Chen, J. E. Bowers, and B. Chen, "High speed mid-wave infrared uni-traveling carrier photodetector," *IEEE J. Quantum Electron.*, vol. 56, no. 4, pp. 1–7, Aug. 2020.

[26] D. Wu, Q. Durlin, A. Dehzangi, Y. Zhang, and M. Razeghi, "High quantum efficiency mid-wavelength infrared type-II InAs/$InAs_{1-x}Sb_x$ superlattice photodiodes grown by metal-organic chemical vapor deposition," *Appl. Phys. Lett.*, vol. 114, no. 1, Jan. 2019, Art. no. 011104, doi: 10.1063/1.5058714.

[27] I. Kimukin, N. Biyikli, T. Kartaloglu, O. Aytur, and E. Ozbay, "High-speed InSb photodetectors on GaAs for mid-IR applications," *IEEE J. Sel. Topics Quantum Electron.*, vol. 10, no. 4, pp. 766–770, Jul./Aug. 2004.